A Closer Look at the Active Site of γ-Class Carbonic Anhydrases: High-Resolution Crystallographic Studies of the Carbonic Anhydrase from *Methanosarcina thermophila*[†,‡]

Tina M. Iverson,[§] Birgit E. Alber,[||,⊥] Caroline Kisker,[@,#] James G. Ferry,[||] and Douglas C. Rees*[,@,$]

Graduate Option in Biochemistry, 147-75CH, California Institute of Technology, Pasadena, California 91125, Department of Biochemistry and Molecular Biology, The Pennsylvania State University, University Park, Pennsylvania 16802, Division of Chemistry and Chemical Engineering, California Institute of Technology, Pasadena, California 91125, and Howard Hughes Medical Institute, Division of Chemistry and Chemical Engineering, 147-75CH, California Institute of Technology, Pasadena, California 91125

Received February 1, 2000; Revised Manuscript Received May 12, 2000

ABSTRACT: The prototype of the γ-class of carbonic anhydrase has been characterized from the methanogenic archaeon *Methanosarcina thermophila*. Previously reported kinetic studies of the γ-class carbonic anhydrase are consistent with this enzyme having a reaction mechanism similar to that of the mammalian α-class carbonic anhydrase. However, the overall folds of these two enzymes are dissimilar, and apart from the zinc-coordinating histidines, the active site residues bear little resemblance to one another. The crystal structures of zinc-containing and cobalt-substituted γ-class carbonic anhydrases from *M. thermophila* are reported here between 1.46 and 1.95 Å resolution in the unbound form and cocrystallized with either SO_4^{2-} or HCO_3^-. Relative to the tetrahedral coordination geometry seen at the active site in the α-class of carbonic anhydrases, the active site of the γ-class enzyme contains additional metal-bound water ligands, so the overall coordination geometry is trigonal bipyramidal for the zinc-containing enzyme and octahedral for the cobalt-substituted enzyme. Ligands bound to the active site all make contacts with the side chain of Glu 62 in manners that suggest the side chain is likely protonated. In the uncomplexed zinc-containing enzyme, the side chains of Glu 62 and Glu 84 appear to share a proton; additionally, Glu 84 exhibits multiple conformations. This suggests that Glu 84 may act as a proton shuttle, which is an important aspect of the reaction mechanism of α-class carbonic anhydrases. A hydrophobic pocket on the surface of the enzyme may participate in the trapping of CO_2 at the active site. On the basis of the coordination geometry at the active site, ligand binding modes, the behavior of the side chains of Glu 62 and Glu 84, and analogies to the well-characterized α-class of carbonic anhydrases, a more-defined reaction mechanism is proposed for the γ-class of carbonic anhydrases.

Carbonic anhydrases are zinc-containing enzymes that were first noted for their physiological role in interconverting CO_2 and HCO_3^- (*1*). On the basis of sequence similarities, there are three distinct classes of carbonic anhydrases: α, β, and γ. The α-class is generally thought of as mammalian, and includes at least 14 mammalian isozymes, along with two isozymes from *Chlamydomonas reinhardtii*, and two prokaryotic isozymes (*2*, *3*). The β-class is primarily found in phototrophic organisms, including plants. The prototype for the γ-class of carbonic anhydrase has been discovered in the methanoarchaeon *Methanosarcina thermophila* (Cam)[1] (*4*). Crystal structures have been reported for Cam (*5*), several isozymes of the α-class of carbonic anhydrase (*6*−*11*), and a β-class of carbonic anhydrase from the red alga *Porphyridium purpureum* (*12*).

In *M. thermophila*, Cam activity increases when the substrate for growth is switched from methanol to acetate (*13*), suggesting involvement of this enzyme in acetate catabolism. *M. thermophila* obtains energy for growth by cleaving the C−C bond of acetate and reducing the methyl

[†] This work was supported by a grant from the National Institutes of Health to J.G.F. (GM44661). T.M.I. is supported by a NIH training grant (GM07737).

[‡] Coordinates for all structures described here have been deposited with the PDB and have been released. The PDB accession numbers are listed in Table 1.

* To whom correspondence should be addressed. E-mail: dcrees@caltech.edu. Phone: (626) 395-8393. Fax: (626) 744-9524.

[§] Graduate Option in Biochemistry, California Institute of Technology.

[||] The Pennsylvania State University.

[⊥] Present address: Institut für Biologie II, Mikrobiologie, Albert-Ludwigs-Universität Freiburg, Schänzlestr. 1, D-79104 Freiburg, Germany.

[@] Division of Chemistry and Chemical Engineering, California Institute of Technology.

[#] Present address: Department of Pharmacological Sciences, State University of New York at Stony Brook, Stony Brook, NY 11794-8651.

[$] Howard Hughes Medical Institute, Division of Chemistry and Chemical Engineering, California Institute of Technology.

[1] Abbreviations: Cam, *M. thermophila* carbonic anhydrase; Zn−Cam, Cam that has been heterologously produced in *Escherichia coli*, metal-depleted, and reconstituted with zinc; Co−Cam, Cam that has been heterologously produced in *E. coli*, metal-depleted, and reconstituted with cobalt; HCAII, human carbonic anhydrase isozyme II; E, enzyme; Bct, bicarbonate; PEG, polyethylene glycol; EXAFS, extended X-ray absorption fine structure; PDB, Protein Data Bank; rms, root-mean-square.

10.1021/bi000204s CCC: $19.00
Published on Web 07/08/2000

group to CH_4 with electrons derived from the oxidation of the carbonyl group to CO_2. It is proposed that CO_2 is converted to HCO_3^- by Cam outside the cell to facilitate either the uptake of acetate or the removal of CO_2 from the cytoplasm. Cam catalyzes the interconversion of CO_2 and HCO_3^- with turnover numbers as high as 6×10^4 s^{-1} (*14*), which approaches the turnover number of 10^6 s^{-1} observed for α-class carbonic anhydrases (*15*).

Kinetic studies (*14*) suggest that the hydration of CO_2 by Cam may occur by a mechanism similar to that proposed for human carbonic anhydrase II (HCAII) (*15*−*18*). HCAII, the best studied carbonic anhydrase and the isozyme with highest activity (*19*), belongs to the α-class of carbonic anhydrases and utilizes a "zinc hydroxide" mechanism for catalysis. The overall enzyme-catalyzed reaction occurs in two distinct half-reactions. The first half-reaction is the interconversion of CO_2 and HCO_3^- (eqs 1a and 1b, where E signifies the enzyme) and involves nucleophilic attack of the zinc hydroxyl ion on CO_2. This is followed by exchange of zinc-bound HCO_3^- with water. The second half-reaction corresponds to the rate-determining intramolecular and intermolecular proton transfer steps (eqs 2a and 2b), which regenerates the zinc hydroxide at the active site.

$$E-Zn^{2+}-OH^- + CO_2 \leftrightarrow E-Zn^{2+}-HCO_3^- \quad (1a)$$

$$E-Zn^{2+}-HCO_3^- + H_2O \leftrightarrow E-Zn^{2+}-H_2O + HCO_3^- \quad (1b)$$

$$E-Zn^{2+}-H_2O \leftrightarrow {}^+H-E-Zn^{2+}-OH^- \quad (2a)$$

$${}^+H-E-Zn^{2+}-OH^- + B \leftrightarrow E-Zn^{2+}-OH^- + BH^+ \quad (2b)$$

The proton indicated in eqs 2a and 2b represents protonation of His 64 of HCAII, which shuttles protons between the active site zinc and the buffer molecules (B) in the solvent (*20*, *21*). Intramolecular proton transfer (eq 2a) is rate-limiting at saturating buffer concentrations. At low buffer concentrations, intermolecular transfer (eq 2b) is rate-limiting.

In addition to the similar kinetic properties, Cam and HCAII exhibit structural similarities in coordination of the zinc ion. The crystal structure of HCAII (*8*) reveals an active site containing a zinc ion tetrahedrally coordinated to three histidines and a highly conserved water molecule. The structure of Cam has been previously determined at 2.8 Å resolution (*5*). Although the overall folds of Cam and HCAII are unrelated, the histidines coordinating the Zn^{2+} ion of Cam superimpose on the corresponding histidines of HCAII. Neighboring residues in the active site of Cam differ completely from those in HCAII, however, and it is not obvious how the residues surrounding the metal site in Cam function, by analogy to catalytically essential residues in HCAII.

One key residue for the catalytic mechanism in HCAII is Thr 199, which has no obvious structurally analogous residue in Cam (*5*). Thr 199 plays two known mechanistic roles. The first is in selecting protonated molecules to bind to the active site zinc. Because of this role, Thr 199 is often termed the "gatekeeper" residue. To achieve this selection, the side chain hydroxyl is hydrogen bonded to the side chain carboxyl of Glu 106, so the Thr 199 OH must be a hydrogen bond donor in that interaction. Consequently, Thr 199 acts as a hydrogen bond acceptor in any other hydrogen bond interactions. Thr 199 OH is directly hydrogen bonded to the Zn-bound water molecule and therefore selects only protonated molecules to bind in that position (*22*). As a result of this directional hydrogen bond, a lone pair of the Zn-bound OH is optimally oriented for attack on CO_2 (*23*). Thr 199 may play other roles in the interconversion of HCO_3^- and CO_2. Crystallographic studies of HCAII with the inhibitors CN^- and CNO^- have shown that, rather than binding to the active site metal as anticipated, both CN^- and CNO^- bind to the backbone amide nitrogen of Thr 199 (*24*). The results from this study suggest that the backbone amide nitrogen of Thr 199 is also involved in catalysis, possibly in both orienting and polarizing the CO_2, preparing it for attack by the Zn-bound OH.

There are also differences in the kinetic behavior of HCAII and Cam. In HCAII, a higher coordination number of the metal ion is postulated to decrease the turnover rate. Indeed, only cobalt-substituted HCAII retains any activity, with 50% of the activity of the native enzyme (*25*). Crystal structures of HCAII metal-substituted with Co, Cu, Ni, or Mn exhibit an increased number of metal-coordinating ligands and longer average coordination distances (*26*), consistent with the theory that the coordination number is a primary factor influencing the turnover rate in HCAII. In contrast to mammalian carbonic anhydrases, substitution of the zinc ion by cobalt doubles Cam activity (*14*), even though EXAFS analysis indicates a higher coordination number for cobalt-substituted Cam (Co−Cam) than for zinc-containing Cam (Zn−Cam). Consequently, while the mechanisms of the α- and γ-classes of carbonic anhydrase enzymes may be similar, they are unlikely to be identical. Further understanding of the similarities and differences of α- and γ-class carbonic anhydrases will help in identifying chemical constraints within which the different classes evolved, and will provide further insight into the fundamental features of the catalytic mechanism of carbonic anhydrases.

The crystal structures of uncomplexed Co−Cam, as well as Co−Cam cocrystallized with HCO_3^- and SO_4^{2-}, were determined at high resolution to investigate whether the change in activity for Co−Cam is an effect of active site coordination, and to learn more about the mechanism of Cam. For accurate comparison to Zn−Cam, high-resolution structures of Zn−Cam, as well as Zn−Cam cocrystallized with HCO_3^- and SO_4^{2-}, have also been determined. These high-resolution structures allow a first look at the solvent structure of the enzyme. As solvent molecules are used as a catalytic group in the reaction, only high-resolution structures can give a complete picture of the active site. These structures allow assignment of several catalytically important residues and solvent molecules in the active site of Cam.

EXPERIMENTAL PROCEDURES

Crystallization. "Cam" refers to native carbonic anhydrase isolated from *M. thermophila* (*13*). "Zn−Cam" and "Co−Cam" designate enzymes in which the indicated metal was incorporated into the active site of the as-purified enzyme produced in *Escherichia coli*, by preparation of the apoenzyme using the denaturant guanidine-HCl and the metal chelator dipicolinate followed by reconstitution in the presence of $ZnSO_4$ or $CoCl_2$ (*14*). For all crystallizations

Table 1: Data Collection and Refinement Statistics[a]

	Zn−Cam	Zn−Cam−HCO_3^-	Zn−Cam−SO_4^{2-}	Co−Cam	Co−Cam−HCO_3^-	Co−Cam−SO_4^{2-}
unit cell ($a = b = c$) (Å)	82.64	82.51	82.68	82.34	82.58	82.61
resolution (Å)	20−1.72	20−1.85	20−1.95	20−1.76	20−1.46	20−1.55
no. of observations	128420	55426	51109	95188	128698	91423
no. of unique reflections	19889	15750	13667	18449	32731	25247
no. of free *R* reflections	1134	937	760	1093	1697	1028
completeness (%)	98.0 (97.6)	96.9 (82.3)	97.5 (95.0)	98.7 (98.7)	99.4 (99.1)	91.5 (90.3)
R_{sym}	0.097 (0.240)	0.050 (0.238)	0.081 (0.284)	0.054 (0.283)	0.055 (0.297)	0.071 (0.276)
I/σ	19 (4.9)	16 (4.3)	14 (4.1)	21 (4.2)	20 (3.2)	15 (3.5)
R_{cryst}	0.189	0.183	0.189	0.181	0.185	0.205
R_{free}	0.227	0.236	0.236	0.217	0.206	0.229
rmsd for bond lengths (Å)	0.021	0.021	0.019	0.011	0.012	0.014
rmsd for bond angles (deg)	1.7	1.8	1.9	1.6	1.6	1.7
coordinate error (Å)	0.12	0.15	0.18	0.12	0.07	0.09
residues	8−213	0−213	6−213	6−213	5−213	8−213
no. of atoms	1617	1674	1601	1641	1681	1629
no. of water molecules	75	64	40	79	118	88
Ramachandran statistics (%)						
most favored regions	90.8	83.4	89.8	89.1	89.8	88.4
allowed regions	9.2	15.5	9.7	9.7	10.2	11.6
generously allowed regions	0	1.1	0.6	0.6	0	0
disallowed regions	0	0	0	0.6 (1)	0	0.6 (1)
PDB entry	1qrg	1qrl	1qrm	1qq0	1qre	1qrf

[a] Numbers in parentheses indicate values for the highest-resolution bin. $R_{sym} = \Sigma_i|I_i - \langle I\rangle|/\Sigma I_i$, where I_i is the *i*th measurement and $\langle I\rangle$ is the weighted mean of *I*. $R_{cryst} = \Sigma||F_o| - |F_c||/\Sigma|F_{obs}|$. R_{free} is the same as R_{cryst} for data omitted from the refinement. The coordinate error is the Cruickshank value (*53*) determined in REFMAC (*31*) and based on the R_{free} value.

described herein, the stock protein concentration is 10 mg/mL buffered in 5 mM phosphate (pH 7.0). Cubic crystals of Zn−Cam were obtained in hanging drops using 3% PEG 8000 and 0.1 M $(NH_4)_2SO_4$ at 22 °C. Cubic crystals of Co−Cam were obtained in hanging drops containing 5% PEG 8000 and 0.5 M $(NH_4)_2SO_4$. The final pH of an artificial crystallization solution was determined to be 6.2. The pH of the crystallization reaction including Co−Cam was determined using a microelectrode to be 5.8. The crystals appeared within 3 days and grew to a maximal size of 0.5 mm × 0.5 mm × 0.5 mm. Cubic crystals belonged to space group $P2_13$ with unit cell dimension *a* being between 82.3 and 82.7 Å and one monomer per asymmetric unit. For cryocooling, all crystals described in this paper were soaked in a solution containing all of the crystallization components along with 25% glycerol.

Cocrystals of Cam with bicarbonate were obtained in hanging drops containing 7.5% PEG 8000, 0.8 M $(NH_4)_2SO_4$, and 20 mM $NaHCO_3$. The crystals were isomorphous with the substrate free crystals. Zn−Cam crystals only formed using PEG 8000 from Hampton, and formation of all bicarbonate cocrystals was dependent on the lot of PEG 8000. This is presumably due to the batch-to-batch variability of chemical impurities in PEG 8000 (*27*).

When the uncomplexed crystals were kept under the crystallization conditions for more than 1 day after crystal formation, a large, unanticipated feature appeared in the electron density maps adjacent to the metal ion. In view of the size and tetrahedral shape of this density, and the fact that $(NH_4)_2SO_4$ was present in the crystallization solution, this density was modeled as SO_4^{2-}.

Data Collection. Data for Zn−Cam complexed with SO_4^{2-}, as well as a low-resolution pass for Zn−Cam, were collected at 113 K using CuKα radiation from an RU 200 rotating anode at a wavelength of 1.54 Å on an Raxis IIc image plate. All other data sets were collected at 93 K at the Stanford Synchrotron Radiation Laboratory beam line 7-1 (λ = 1.08 Å) using a MAR Research image plate detector. All data were processed using DENZO and scaled with SCALEPACK (*28*). The resolutions of the data sets merged from 1.46 to 1.95 Å (Table 1).

The structure of Co−Cam was determined by molecular replacement in AMORE (*29*) using the Cam monomer (*5*) as a search model. The other cubic crystals of Cam were isomorphous with cubic Co−Cam. Therefore, the refined monomer of Co−Cam from the cubic space group was used as a starting model in those cases.

Model Building and Refinement. All Cam models were built using the program O (*30*). Refinement was carried out using REFMAC (*31*, *32*) and X-PLOR (*33*). Uncomplexed structures were first refined with bond lengths of the metal coordinating ligands restrained to the distances determined by EXAFS (*14*). After the R_{cryst} dropped below 19%, the refinement proceeded unrestrained. The R_{free} was composed of 1093 randomly selected reflections from the native Co−Cam data set (6%). The reflections for R_{free} for the remaining data sets are identical to those from the Co−Cam data set with additional randomly selected reflections selected for higher-resolution data sets. PDB accession codes and statistics are given in Table 1.

RESULTS

Overall Fold of the Enzyme

The overall fold of Zn−Cam is a left-handed β-helix (Figure 1) as previously reported (*5*). Superposition of residues 9−213 of the monomers of Zn−Cam and Co−Cam resulted in an overall rms deviation of 0.22 Å and an rms deviation for the residues in the β-helix of 0.14 Å, indicating that no significant overall structural change occurs upon metal substitution. When a trimer of Zn−Cam from the previously reported tetragonal space group ($P4_32_12$) (*5*) was superimposed onto a trimer of Co−Cam, the rms deviation was 0.37 Å for the C_α atoms of residues 6−212 and 0.23 Å

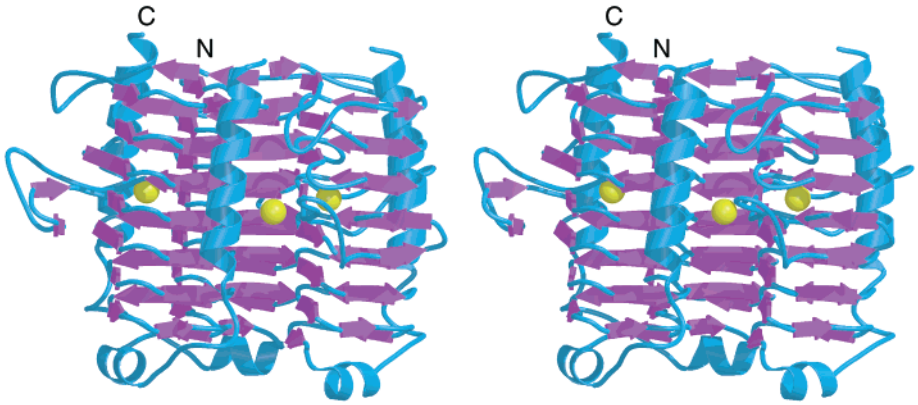

FIGURE 1: Stereoview illustrating the Cam trimer. The overall fold is a left-handed β-helix, consisting of three untwisted, parallel β-sheets connected by left-handed crossovers. This figure was made using MOLSCRIPT (*49*), BOBSCRIPT (*50*), and RASTER3D (*51*).

for the C_α atoms of residues of the β-helix. Thus, with the exception of the N-termini described below, no significant structural changes occur in the trimer with the change in space group.

The structure of Zn−Cam in the tetragonal space group (*5*) shows two trimers related by a 2-fold axis with an interaction between the N-termini (residues 0−6) creating a six-stranded β-barrel. In cubic space group $P2_13$, there is no 2-fold axis relating the trimers, indicating that Cam forms a trimer and not a hexamer in the crystal. In the model of Zn−Cam in complex with HCO_3^-, the N-termini are lying across the top of the trimer in an extended conformation. However, in the remainder of the models, the N-termini are disordered.

Active Site

As previously described (*5*), the active site contains a zinc ion coordinated to the protein by three histidine side chains. In the structures described here, the active site coordination geometry differs depending on the divalent cation at the metal center and the presence or absence of additional ligands. The coordination geometry relative to the metal center is summarized in Table 2.

Active Site of Uncomplexed Zn−Cam. In the active site of uncomplexed Zn−Cam, the Zn^{2+} has three protein and two solvent ligands arranged in trigonal bipyramidal geometry (Figure 2A and Table 3). As was determined previously for Cam (*5*), the zinc is coordinated between two monomers with His 81 and His 122 contributed by one monomer, and His 117 contributed from an adjacent monomer. In the previously described structure, only one Zn-bound water molecule was identified, due to difficulties in conclusively assigning water molecules at 2.8 Å resolution. The water molecule assigned in the 2.8 Å resolution structure corresponds to Wat 2 in the high-resolution structure of Zn−Cam.

In this high-resolution study, an additional solvent molecule coordinating the zinc ion could be identified in the electron density maps. The coordination geometry for the Zn^{2+} is summarized in Table 3. Pentacoordination is consistent with the EXAFS data, which show a Zn^{2+} coordination sphere of $Zn(N,O)_{2-3}(imidazole)_3$ (*14*). The average bond distance of 2.14 Å is within experimental error of the distance determined by EXAFS of 2.06 Å, where the errors in the EXAFS determination are approximately 0.02 Å and the coordinate errors for the crystal structures are listed in Table 1.

Table 2: Summary of Metal Ligation in Cam

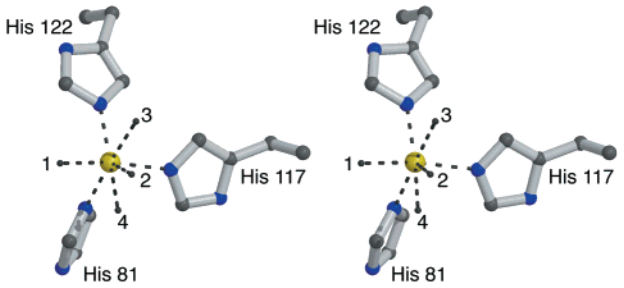

	ligation position 1	ligation position 2	ligation position 3	ligation position 4
Zn−Cam uncomplexed	Wat 1	Wat 2	x	x
Co−Cam uncomplexed	Wat 1	x	Wat 2	Wat 3
Zn−Cam−HCO_3^-	HCO_3^- O3	HCO_3^- O1[a]	x	x
Co−Cam−HCO_3^-	Wat 1	x	Wat 2	HCO_3^- O1
Zn−Cam−SO_4^{2-}	SO_4^{2-} O4	SO_4^{2-} O3	x	x
Co−Cam−SO_4^{2-}	SO_4^{2-} O4	SO_4^{2-} O3	x	Wat 36*

[a] This denotes a significant shift in the ligation position relative to the uncomplexed form. In the Zn−Cam−HCO_3^- complex, the HCO_3^- O1 is displaced 1.5 Å relative to the location of the water molecule in Zn−Cam. In the Co−Cam−SO_4^{2-} complex, water 36 is displaced 0.9 Å from the location of Wat 3 in uncomplexed Co−Cam. Of note is the fact that Co−Cam and Zn−Cam always fill ligation position 1, while ligation position 2 tends to be occupied in Zn−Cam (resulting in trigonal bipyramidal coordination geometry) and ligation positions 3 and 4 tend to be occupied in Co−Cam (resulting in octahedral geometry). The exception is Co−Cam−SO_4^{2-} which fills ligation positions 1, 2, and 4, resulting in a more distorted coordination geometry.

An interesting aspect of these structures is the multiple conformations for the side chain of Glu 84. In Zn−Cam, two discrete conformations of Glu 84 are present, one of which points toward the active site and lies within hydrogen-bonding distance of the side chain of Glu 62. In the other structures described in this paper, a third conformation for the side chain of Glu 84 was observed (Figure 3A). Since the side chains of Glu 84 and Glu 62 lie within hydrogen-bonding distance of each other, it is likely that a proton lies between these two side chains. This indicates that the protein environment has elevated the pK_a value for one or both of these side chains above that observed in solution. The observation further suggests that protons may be shuttled out of the active site via a mechanism involving both Glu 62 and Glu 84. Glu 84 may be analogous to the proton shuttle residue His 64 of HCAII (Figure 3B), which exhibits two discreet conformations in the crystal structure (*34*). Replace-

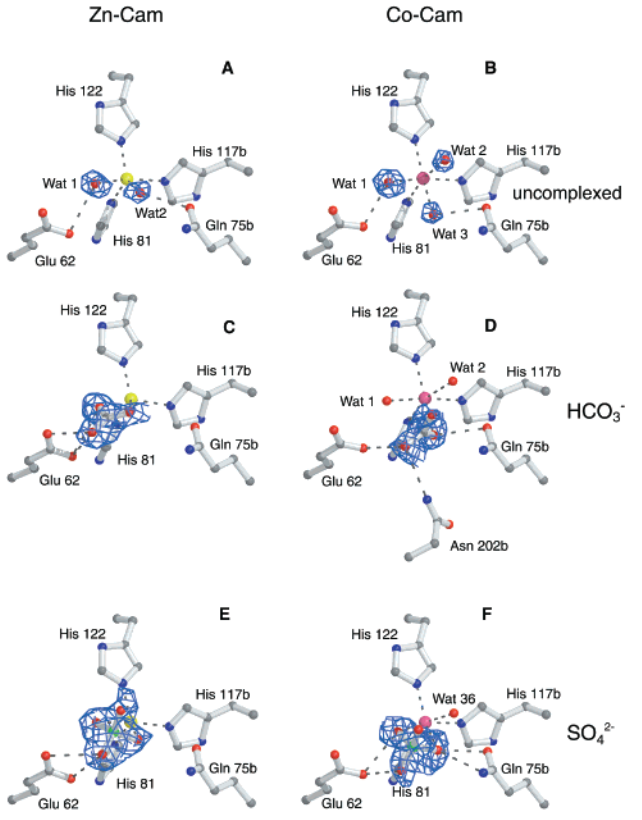

FIGURE 2: Active site coordination. Models are superimposed onto $|F_o| - |F_c|$ omit maps calculated after the removal of the relevant active site ligands and contoured at 4σ. (A) The coordination of Zn−Cam exhibits distorted trigonal bipyramidal geometry. (B) The coordination of Co−Cam exhibits distorted octahedral geometry. (C) The coordination of Zn−Cam bound to bicarbonate. (D) The model of Co−Cam bound to HCO_3^-. (E) The model of Zn−Cam bound to SO_4^{2-}. (F) The model of Co−Cam bound to SO_4^{2-}. This figure was made using MOLSCRIPT (*49*), BOBSCRIPT (*50*), and RASTER3D (*51*).

Table 3: Active Site Geometry of Zn−Cam

atom	distance to zinc (Å)	x−Zn−W2 (deg)	x−Zn−81 (deg)	x−Zn−117 (deg)	x−Zn−122 (deg)
Wat 1	2.14	71.9	92.8	161.4	93.1
Wat 2	2.13		121.4	90.1	119.1
His 81	2.15			118.0	92.3
His 117	2.23				100.3
His 122	2.06				
average	2.14				

ment of Glu 84 with alanine in Cam decreases protein activity to 1% of wild-type levels, and this activity is restored to 53% of wild-type activity by the addition of imidazole (*35*). Imidazole has been shown to act as an alternative proton shuttle in HCAII (*21*), lending biochemical support to the crystallographic observation that Glu 84 may act as a proton shuttle in Cam.

Active Site of Uncomplexed Co−Cam. The active site of Co−Cam shows that the cobalt is hexacoordinate in a distorted octahedral arrangement, with ligands provided by the three histidine side chains and three water molecules (Figure 2B and Table 4). Hexacoordination is consistent with the EXAFS data that suggest $Co(N,O)_{2-3}(imidazole)_{2-3}$ coordination (*14*). Only one of the three water molecules (Wat 1) coordinating the cobalt corresponds to a water molecule (Wat 1) coordinating the zinc in Zn−Cam (Table 2). Thus, Wat 2 of Zn−Cam and Wat 2 and Wat 3 of Co−Cam are unique to each structure. In contrast, almost 70% of the water molecules not located in the active site have equivalent locations in these two uncomplexed structures.

The average Co^{2+}−ligand bond length of 2.32 Å observed for Co−Cam is similar to the average ligation distance of 2.2 Å observed for other six-coordinate Co^{2+} in protein structures (*36*−*40*). The average Co−ligand bond length determined by EXAFS analysis of Co−Cam is 2.09 Å (*14*), and the disagreement in bond lengths is just outside of the experimental error of both techniques. This disagreement may arise from pH differences between the crystallization conditions (pH 5.8) and EXAFS conditions (pH 7.0). In HCAII, lowered pH lengthens metal−ligand bonds (*8*, *26*, *41*) so that a comparison of ligation bond lengths may not be accurate when the pHs of the buffers differ.

Active Site of Zn−Cam Cocrystallized with Bicarbonate. Crystallographically, carbonic acid (H_2CO_3) and bicarbonate (HCO_3^-) are indistinguishable at the resolution of these structures. Although HCO_3^- was added the crystallization conditions, the species bound to the active site might be H_2CO_3 rather than HCO_3^-. First, the pH of the crystallization conditions is very near the pK_a of bicarbonate, so protonation may have occurred in solution. Second, the pK_a of bicarbonate could be elevated when it is bound to the protein, as appears to be the case for the neighboring Glu 62 and Glu 84 side chains. Third, HCO_3^- has a very low affinity for the enzyme, similar to that of HCAII. In HCAII, it has not been possible so far to cocrystallize the native enzyme with the substrate due to the weak binding. The cocrystallization of bicarbonate with cobalt-substituted HCAII (*42*) and two forms of the enzyme that had been made less active by site-specific replacement of Thr 199 or Thr 200 (*22*, *43*) each show different binding modes for bicarbonate at the active site. The cobalt-substituted enzyme (*42*) and the enzyme where Thr 200 has been replaced (*43*) each display bidentate ligation, while the enzyme with Thr 199 genetically altered (*22*) shows monodentate ligation, leading to the suggestion that bicarbonate binds to the HCAII active site in a continuum of modes (*44*, *45*). Although the carbonic acid concentration is only 0.1% as large as that of CO_2 at equilibrium in solution, it is possible that H_2CO_3 might have stable contacts in the Cam active site, which could facilitate trapping of this nonproductive complex in the crystal.

The hydrogen-bonding contacts of the species observed at the active site cannot unambiguously identify the nature of the ligand. The ligand has three oxygens within hydrogen-bonding distance (<3.2 Å) of the side chain of Glu 62. It is not possible, however, to establish the location and nature of the bound protons, since the potential hydrogen bonds are not optimally oriented. Furthermore, it is possible that the interaction between the side chain of Glu 62 and the active site ligand is primarily electrostatic, where the partial positive charge of one hydrogen stabilizes multiple oxygen−oxygen contacts. For the purposes of describing the interaction, the species will be termed bicarbonate (HCO_3^-), despite its ambiguous identity.

Bicarbonate binds in a bidentate fashion to the Zn^{2+}, replacing both Wat 1 and Wat 2 (Figure 2C and Table 5). The HCO_3^- is stabilized by the coordination of one oxygen (O3) directly to the active site zinc and by a hydrogen bond contact of this same oxygen (O3) to the side chain of Glu

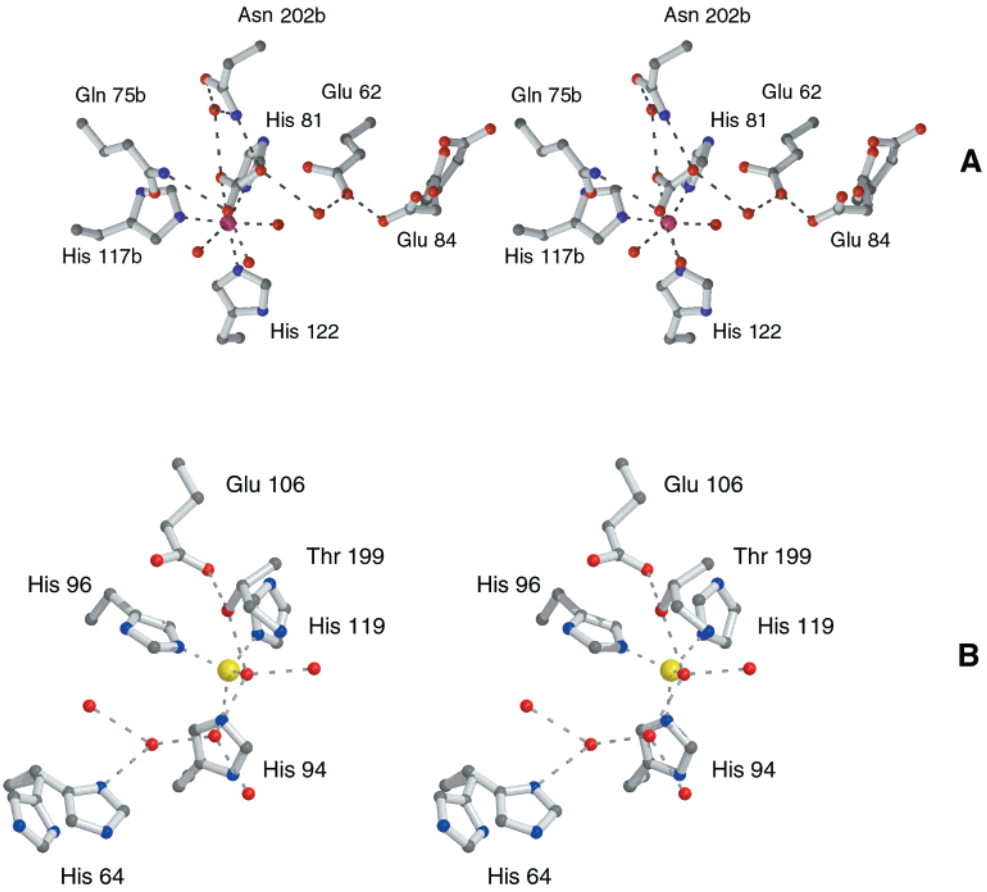

FIGURE 3: (A) Stereoview of some catalytically important residues. The active site of Co−Cam in complex with HCO_3^- is shown with residues that may be functionally important. The hydrogen bonds between HCO_3^- and the candidates for a Thr 199 analogue (Gln 75b and Asn 202b) are shown. Glu 84 is shown in three conformations, two of which are alternative conformations in the Zn−Cam structure, while the third conformation is present in the remaining structures. (B) Stereoview of the active site of HCAII. The view is shown with the metal-ligating histidines in the same relative orientation as in panel A; i.e., His 119 of HCAII, which coordinates using the Nδ atom, is shown in the same relative location as His 81 of Cam, which also ligates the metal using the Nδ atom. His 64, which is thought to act as the proton shuttle, is shown in both conformations. This figure was made using MOLSCRIPT (*49*), BOBSCRIPT (*50*), and RASTER3D (*51*).

Table 4: Active Site Geometry of Co−Cam

atom	distance to cobalt (Å)	x−Co−W2 (deg)	x−Co−W3 (deg)	x−Co−81 (deg)	x−Co−117 (deg)	x−Co−122 (deg)
Wat 1	2.31	90.9	81.2	89.4	169.0	91.0
Wat 2	2.50		82.4	169.6	84.7	82.5
Wat 3	2.42			87.4	88.2	162.8
His 81	2.29				93.2	107.9
His 117	2.19					98.4
His 122	2.25					
average	2.32					

Table 5: Active Site Geometry of Zn−Cam Complexed with HCO_3^-

atom	distance to zinc (Å)	x−Zn−Bct O1 (deg)	x−Zn−81 (deg)	x−Zn−117 (deg)	x−Zn−122 (deg)
Bct O3	2.27	45.9	92.8	152.0	94.9
Bct O1	3.24		121.2	110.1	106.2
His 81	2.18			90.3	119.2
His 117	2.30				107.8
His 122	2.05				
average	2.41 (2.2 Å without Bct O1)				

62. A second bicarbonate oxygen (O1) makes a long contact with the Zn^{2+}. The third oxygen (O2) is within hydrogen-bonding distance of both carboxylate oxygens of the Glu 62 side chain.

Active Site of Co−Cam Cocrystallized with Bicarbonate. HCO_3^- binds in a monodentate fashion to the cobalt, replacing one of the coordinating water molecules (Wat 3 from Co−Cam) as well as a second water molecule (Wat 4

Table 6: Active Site Geometry of Co−Cam Complexed with HCO_3^-

atom	distance to cobalt (Å)	x−Co−W2 (deg)	x−Co−Bct (deg)	x−Co−81 (deg)	x−Co−117 (deg)	x−Co−122 (deg)
W1	2.25	98.0	78.3	89.3	172.5	88.0
W2	2.31		78.9	162.5	81.8	87.4
BctO1	2.35			87.1	94.3	159.0
His81	2.22				89.0	108.9
His117	2.30					99.4
His122	2.19					
average	2.27					

Table 7: Active Site Geometry of Zn−Cam Complexed with SO_4^{2-}

atom	distance to zinc (Å)	x−Zn−O3 (deg)	x−Zn−81 (deg)	x−Zn−117 (deg)	x−Zn−122 (deg)
SO_4 O4	2.40	62.7	98.3	163.3	85.9
SO_4 O3	2.17		117.1	100.7	122.9
His 81	2.17			90.1	113.4
His 117	2.30				104.1
His 122	2.11				
average	2.23				

from Co−Cam) that is part of a water molecule network in the active site (Figure 2D and Table 6). The water molecule replaced in the Co−Cam−HCO_3^- complex is not present in Zn−Cam, so the HCO_3^- binding differs between Zn−Cam and Co−Cam. Multiple binding modes of HCO_3^- suggest that the active site cavity can accommodate a continuum of binding modes for the substrate, as is proposed for HCAII (*45*, *46*). The ligand is partially stabilized in this binding mode by a hydrogen bond contact with the side chain of Glu 62.

Active Site of Zn−Cam in Complex with Sulfate. Sulfate has been shown not to inhibit Cam activity at concentrations up to 0.3 M at pH 5.9 (B. Tripp and J. G. Ferry, unpublished results). Therefore, it was surprising to find that in Cam, sulfate can bind directly to the Zn^{2+} in a manner suggestive of an inhibitor. The binding replaces both zinc-coordinating waters and thus retains the distorted trigonal bipyramidal coordination (Figure 2E and Table 7). One oxygen (O1) is within hydrogen-bonding distance of the side chain of Glu 62. This suggests that a proton is shared between the side chain of Glu 62 and the active site ligand, and further supports an elevation of the pK_a value for the Glu 62 side chain.

Active Site of Co−Cam Complexed with Sulfate. In the complex of Co−Cam and SO_4^{2-}, the SO_4^{2-} binds to the cobalt in a bidentate fashion, replacing Wat 1 and Wat 3, but retaining Wat 2 (Figure 2F and Table 8). Although the SO_4^{2-} contacts the side chain of Glu 62 as in the Zn−Cam−SO_4^- complex, in the Co−Cam−SO_4^{2-} structure, there are two contacts within hydrogen-bonding distance, rather than one. It is possible that these two contacts are sharing a single proton, most likely donated by a protonated Glu 62.

DISCUSSION

Reaction Mechanism Implications. As discussed above, kinetic analyses indicate that Cam and HCAII each catalyze the interconversion of CO_2 and HCO_3^- through a zinc hydroxide mechanism (*14*). Comparison of the active site structures of Cam and HCAII highlights side chains that may function analogously in these two enzymes. As HCAII has been extensively studied, this comparison helps construct a preliminary structure-based mechanism for Cam. Differences in the active sites are also of interest as they highlight aspects of the reaction mechanism that have evolved to proceed using different components, yet are still compatible with high rates in both cases.

In the first half-reaction (eqs 1a and 1b), a metal-bound hydroxyl group directly attacks CO_2. In HCAII, it is proposed that CO_2 binds in a hydrophobic pocket of the active site lined with the side chains of Val 121, Val 143, Leu 198, and Trp 209 (*47*). The active site of Cam is located at the base of a cleft between the two monomers. An electrostatic surface potential representation (Figure 4) shows the HCO_3^- from the Zn−Cam−HCO_3^- complex appears to be solvent accessible. Below the active site cavity of Cam, there appears to be a relatively apolar surface (Figure 4). This surface, composed of the side chains of Leu 83, Phe 132b (where b denotes that the residue belongs to the adjacent monomer), Met 135b, Phe 138, Phe 140, Ile 157, and Val 172, may be analogous to the hydrophobic pocket in HCAII, thus serving as a binding site for CO_2 in the active site.

In HCAII, following the trapping of CO_2 by the hydrophobic pocket, CO_2 may interact with the amide nitrogen of Thr 199 (*24*, *48*), replacing the deep water molecule (*8*). In the Co−Cam−HCO_3^- structure, Gln 75b Nϵ and Asn 202b Nδ serve as hydrogen bond donors for O2 and O3 of the metal-bound HCO_3^- (Figure 3A). However, they do not contact the HCO_3^- in the Zn−Cam−HCO_3^- structure. These two residues are possible candidates for orienting CO_2 for attack or stabilizing a transition state. Since the active site solvent structure is very different in Zn−Cam and Co−Cam, candidates for a deep water molecule are less clear. Although water molecules are missing from each structure upon binding of HCO_3^- (Wat 4 from Co−Cam and Wat 24 from Zn−Cam), these water molecules are not analogous.

In HCAII, the first half-reaction culminates in the formation of a bond between the metal-bound OH and the CO_2 to form metal-bound HCO_3^-, followed by an exchange of the HCO_3^- with water (eq 1b). During this transition state, the side chain of Thr 199 helps orient the product. Although an exact analogue of Thr 199 does not exist in Cam, Glu 62 does act to stabilize the binding of ligands to the active site, and thus could partially fulfill a gatekeeper function. Studies of HCAII have previously suggested that bicarbonate may isomerize to form a leaving group (*44*). Multiple binding modes for HCO_3^- in the active site of Cam suggest there may be a continuum of binding modes available to the substrate, and perhaps that isomerization could occur before product release.

Active site coordination has been postulated to be a primary factor in determining the first committed step of catalysis by HCAII (eqs 1a and 1b) (*8*, *49*). The most obvious

Table 8: Active Site Geometry of Co−Cam Complexed with SO_4^{2-}

atom	distance to cobalt (Å)	x−Co−O3 (deg)	x−Co−O4 (deg)	x−Co−81 (deg)	x−Co−117 (deg)	x−Co−122 (deg)
Wat 1	2.29	55.5	91.7	153.0	76.5	92.4
SO_4 O3	2.32		64.2	103.8	94.2	141.4
SO_4 O4	2.09			93.6	158.3	100.2
His 81	2.14				89.3	112.7
His 117	2.31					98.4
His 122	2.13					
average	2.21					

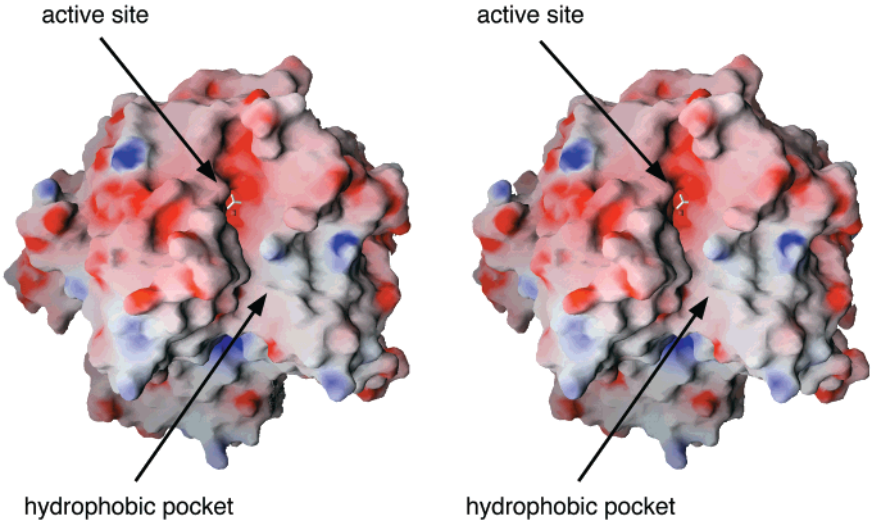

FIGURE 4: Stereoview of a electrostatic surface potential representation calculated using the program GRASP (*52*) at an ionic strength of 100 mM and contoured at $\pm 12 k_B T$ (k_B is the Boltzmann constant and T is the absolute temperature). The N-terminus of the protein is at the top of the representation. The surface was made from the Zn−Cam−HCO_3^- trimer with the bicarbonate omitted and shows that the active site cavity is weakly negatively charged. The HCO_3^- is shown as a stick representation. Directly below the active site cavity (lower right) is a funnel-shaped hydrophobic pocket, which may serve to trap CO_2 into the active site. The negatively charged tunnel above the active site contains Glu 62 and Glu 84, and is believed to be the proton shuttle pathway. The view is the same as in Figure 1.

structural similarity between the α- and γ-classes of carbonic anhydrase is the conserved metal coordination by three histidines. Two of the histidines use Nϵ for metal coordination, while the third uses Nδ (Figure 3A,B). However, as discussed above, solvent ligation of the metal center of Cam differs from HCAII with respect to the water ligands. Both native Zn-containing HCAII and Co-substituted HCAII have distorted tetrahedral geometries, while Zn−Cam is trigonal bipyramidal and Co−Cam octahedral. The active site coordination and geometry in Zn−Cam most closely resemble those of Ni-substituted HCAII, while the geometry of Co−Cam most closely resembles that of Mn-substituted HCAII (*26*). Both Ni- and Mn-substituted HCAII are essentially inactive enzymes. It is a fascinating mystery why the Cam-catalyzed reaction proceeds at a high rate with an increased number of active site ligands relative to HCAII, and dramatically illustrates the complexity of protein−solvent−metal interactions and their implications for reaction mechanisms.

In HCAII, the second half-reaction (eqs 2a and 2b) contains the proton transfer step, which shuttles a proton from the metal-bound water molecule into the solvent, regenerating the metal hydroxide active site. Residues that potentially act analogously in HCAII and Cam are more clear for this half-reaction. The proton shuttle His 64 of HCAII has two discrete conformations in the crystal structure (*34*). In this ensemble of structures, Glu 84 has three discrete conformations, and in one of those conformations, a proton apparently is shared between the side chains of Glu 62 and Glu 84 (Figure 3). Glu 62 and Glu 84 are located at the base of the active site in a negatively charged tunnel (Figure 4) which may aid in the protein−solvent transfer of protons. The direct contact between Glu 84 and Glu 62, combined with the likely protonation of Glu 62 when a ligand is bound to the active site, suggests that the proton shuttle involves both side chains. However, a proton could alternatively be shuttled from the active site to Glu 84 through an intervening water molecule (Wat 67 in Zn−Cam) that provides a hydrogen bond bridge between the active site ligands and the side chain of Glu 84.

On the basis of the finding in this study, as well as previous biochemical evidence, a preliminary reaction mechanism is proposed (Figure 5) which provides a foundation for future studies. This mechanism is missing aspects that are involved in the first half-reaction as they cannot be determined conclusively with the findings to date. In the proposed mechanism, CO_2 binds adjacent to the zinc-bound hydroxyl (representations A and B), the position of which is unknown. The hydroxyl attacks CO_2, leading to a transition state in which the protonated oxygen of the bicarbonate is coordinated to the metal, possibly stabilized by either Gln 75 or Asn 202. These steps are primarily based on analogy to the well-characterized HCAII and a kinetic analysis of Cam, suggesting a zinc hydroxide mechanism. The subsequent steps are based on structures revealed by this study. In the next step, the bicarbonate may isomerize (representations C and D) before replacement by a water molecule (representa-

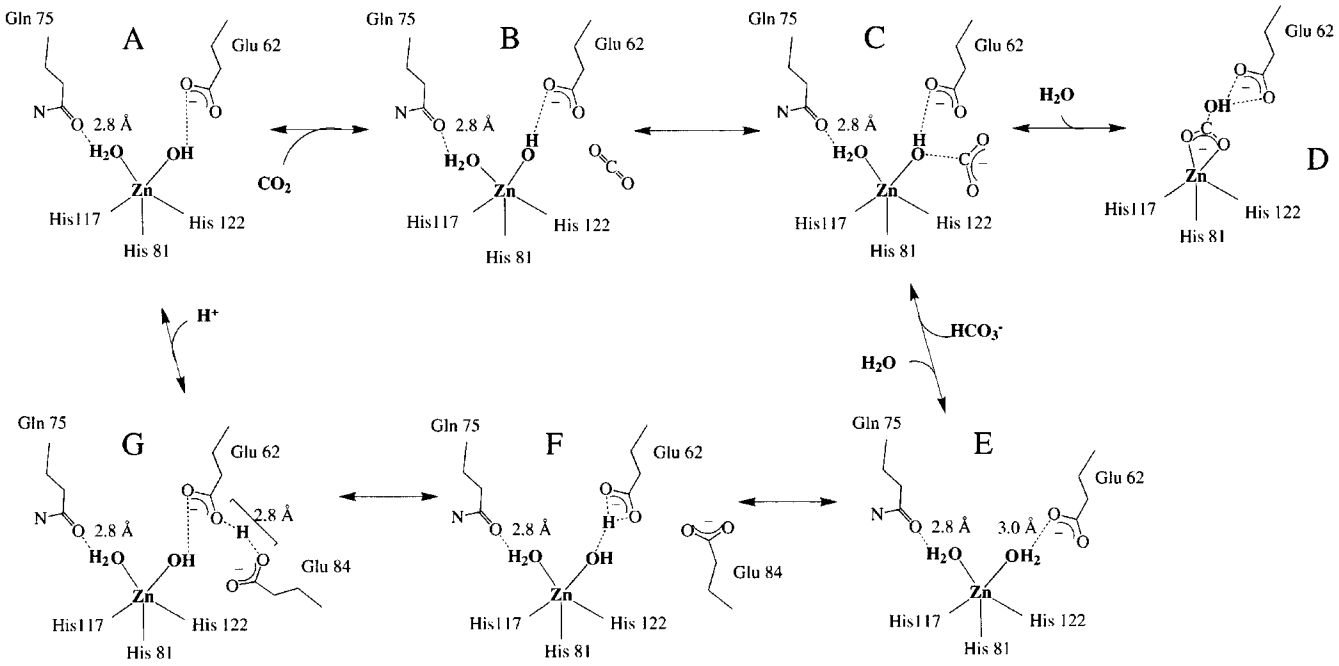

FIGURE 5: Proposed reaction mechanism for Cam. The reaction mechanism is drawn using Zn−Cam as the template. Co−Cam should have a similar reaction mechanism with an additional water molecule as an active site ligand. (A) Zn^{2+} is coordinated to one water molecule and one hydroxide ion at the beginning of the first half-reaction (eqs 1a and 1b). (B) Carbon dioxide enters the active site along the hydrophobic pocket. (C) Carbon dioxide is attacked by the hydroxide bound to the zinc. (D) The bicarbonate may have several stable binding modes. This bidentate binding mode, which requires loss of a metal ligand water molecule, is similar to that seen in the structure of Zn−Cam in complex with HCO_3^-. (E) The first half-reaction ends with exchange of bicarbonate and a water molecule from the solvent. This state is crystallographically indistinguishable from that shown in state A, and may be represented by the structures of Zn−Cam or Co−Cam. (F) The second half-reaction (eqs 2a and 2b) begins with the deprotonation of one zinc-bound water molecule, with the proton transferred to Glu 62. During this process, the side chain of Glu 84 swings in so that it may accept the proton. This step is represented by the structure of water-liganded Zn−Cam with the Glu 84 side chain in conformation 1. (G) The proton is passed from Glu 62 to Glu 84. This state is represented by the structure of Zn−Cam with the Glu 84 side chain in conformation 2. With the transfer of proton to the solvent, the second half-reaction is complete and state A is regenerated.

tion E). In the final steps, Glu 62 shuttles a proton from one of the metal-bound water molecules, transferring it to Glu 84 and regenerating the active zinc-bound hydroxyl (representations F and G).

Summary and Conclusions. This study, presenting a high-resolution structure for Zn−Cam and the first structure of the Co-substituted Cam, has advanced our structural and functional understanding of the prototype of the novel γ-class of carbonic anhydrases. The results identify five and six coordinate metals in Zn−Cam and Co−Cam, a distinct departure from the active site coordination of the α-class of carbonic anhydrases. The high-resolution structures also identify active site water molecules involved in both metal ligation and the hydrogen-bonding network with adjacent residues that are likely to be catalytically important. The structures presented here have identified multiple positions for Glu 84, consistent with a role for this residue in proton transfer from the zinc-bound water molecule to bulk solvent.

The results presented here also raise questions concerning the mechanism of Cam. For example, many of the active site residues (Glu 62, Glu 84, and Asn 202) are poorly conserved between Cam and homologues whose sequences are significantly similar to that of Cam, which is surprising since these appear to be critical for the catalytic mechanism of Cam (*35*). However, to date none of these homologous proteins have yet been shown to actually exhibit carbonic anhydrase activity. Additionally, there are several residues near the active site that are well-conserved in homologues (Arg 59, Asp 61, and Gln 75) where it is unclear how they function in the catalytic mechanism. The results identify residues that potentially function in proton transport; however, residues with the potential to function in CO_2 hydration have yet to be identified. Crystallographic analysis of inhibitor complexes may suggest the location of the CO_2 binding site. Site-directed mutagenesis is expected to identify residues essential for the first half-reaction and the so-called gatekeeper function; indeed, this study has suggested Gln 75 and Asn 202 as potential targets for site-specific replacement.

ACKNOWLEDGMENT

We are grateful to C. Fierke, D. Silverman, and R. Cheng for critical reading and helpful discussions, B. Tripp for unpublished results, and H. Schindelin for experimental assistance. This work is based upon research conducted at the Stanford Synchrotron Radiation Laboratory (SSRL), which is funded by the Department of Energy, Office of Basic Energy Sciences.

NOTE ADDED IN PROOF

The structure of the β-class carbonic anhydrase from *Pisum sativum* was recently reported (*54*).

REFERENCES

1. Meldrum, H., and Roughton, F. (1933) *J. Physiol. 80*, 113−142.
2. Hewett-Emmett, D., and Tashian, R. (1996) *Mol. Phylogenet. Evol. 5*, 50−77.

3. Soltes-Rak, E., Mulligan, M. E., and Coleman, J. R. (1997) *J. Bacteriol. 179*, 769−774.
4. Alber, B. E., and Ferry, J. G. (1994) *Proc. Natl. Acad. Sci. U.S.A. 91*, 6909−6913.
5. Kisker, C., Schindelin, H., Alber, B. E., Ferry, J. G., and Rees, D. (1996) *EMBO J. 15*, 2323−2330.
6. Kannan, K. K., Notstrand, B., Fridborg, K., Lövgren, S., Ohlsson, A., and Petef, M. (1974) *Proc. Natl. Acad. Sci. U.S.A. 72*, 51−55.
7. Kannan, K., Ramanadham, M., and Jones, T. (1984) *Ann. N.Y. Acad. Sci. 429*, 49−60.
8. Håkansson, K., Carlsson, M., Svensson, L. A., and Liljas, A. (1992) *J. Mol. Biol. 227*, 1192−1204.
9. Eriksson, A. E., and Liljas, A. (1993) *Proteins: Struct., Funct., Genet. 16*, 29−42.
10. Boriack-Sjodin, P. A., Heck, R. W., Laipis, P. J., Silverman, D. N., and Christianson, D. W. (1995) *Proc. Natl. Acad. Sci. U.S.A. 92*, 10949−10953.
11. Stams, T., Nair, S. K., Okuyama, T., Waheed, A., Sly, W. S., and Christianson, D. W. (1996) *Proc. Natl. Acad. Sci. U.S.A. 93*, 13589−13594.
12. Mitsuhasi, S., Mizushima, T., Yamashita, E., Yamamoto, M., Kumasaka, T., Moriyana, H., Ueki, T., Miyachi, S., and Tsukihara, T. (2000) *J. Biol. Chem. 275*, 5521−5526.
13. Alber, B. E., and Ferry, J. G. (1996) *J. Bacteriol. 178*, 3270−3274.
14. Alber, B. E., Colangelo, C. M., Dong, J., Stålhandske, C. M. V., Baird, T. T., Tu, C., Fierke, C. A., Silverman, D. N., Scott, R. A., and Ferry, J. G. (1999) *Biochemistry 38*, 13119−13128.
15. Silverman, D. N., and Lindskog, S. (1988) *Acc. Chem. Res. 21*, 30−36.
16. Khalifah, R. G. (1971) *J. Biol. Chem. 246*, 2561−2573.
17. Steiner, H., Jonsson, B. H., and Lindskog, S. (1975) *Eur. J. Biochem. 59*, 253−259.
18. Christianson, D. W., and Fierke, C. A. (1996) *Acc. Chem. Res. 29*, 331−339.
19. Sly, W. S., and Hu, P. Y. (1995) *Annu. Rev. Biochem. 64*, 375−401.
20. Taoka, S., Tu, C. K., Kistler, K. A., and Silverman, D. N. (1994) *J. Biol. Chem. 269*, 17988−17992.
21. Tu, C. K., Silverman, D. N., Forsman, C., Jonsson, B. H., and Lindskog, S. (1989) *Biochemistry 28*, 7913−7918.
22. Xue, Y., Liljas, A., Jonsson, B.-H., and Lindskog, S. (1993) *Proteins: Struct., Funct., Genet. 17*, 93−106.
23. Merz, K. M. (1990) *J. Mol. Biol. 214*, 799−802.
24. Lindahl, M., Svensson, L. A., and Liljas, A. (1993) *Proteins: Struct., Funct., Genet. 15*, 177−182.
25. Hunt, J., Rhee, M., and Storm, C. (1977) *Anal. Biochem. 79*, 614−617.
26. Håkansson, K., Wehnert, A., and Liljas, A. (1994) *Acta Crystallogr. D50*, 93−100.
27. Jurnak, F. (1986) *J. Cryst. Growth 76*, 577−582.
28. Otwinowski, Z. (1993) in *CCP4 Study Weekend Data Collection and Processing* (Sawyer, L., Isaacs, N., and Bailey, S., Eds.) pp 56−62, SERC Daresbury Laboratory, Warrington, U.K.
29. Navaza, J. (1994) *Acta Crystallogr. A50*, 157−163.
30. Jones, T. A., Zou, J. Y., Cowan, S. W., and Kjeldgaard, M. (1991) *Acta Crystallogr. A47*, 110−119.
31. Bailey, S. (1994) *Acta Crystallogr. D50*, 760−763.
32. Murshudov, G. N., Vagin, A. A., and Dodson, E. J. (1997) *Acta Crystallogr. D53*, 240−255.
33. Brünger, A. T. (1992) *X-PLOR version 3.1: A system for X-ray crystallography and NMR*, Yale University Press, New Haven, CT.
34. Nair, S. K., and Christianson, D. W. (1991) *J. Am. Chem. Soc. 113*, 406−411.
35. Tripp, B., and Ferry, J. (2000) *Biochemistry 39*, 9232−9240.
36. Jenkins, J., Janin, J., Rey, F., Chiadmi, M., vanTilbeurgh, H., Lasters, I., DeMaeyer, M., VanBelle, D., Wodak, S. J., Lauwereys, M., Stanssens, P., Mrabet, N. T., Snauwaert, J., Matthysens, G., and Lambeir, A. (1992) *Biochemistry 31*, 5449−5458.
37. Lloyd, L. F., Gallay, O. S., Akins, J., and Zeikus, J. G. (1994) *J. Mol. Biol. 240*, 504−506.
38. Holland, D. R., Hausrath, A. C., Juers, D., and Matthews, B. W. (1995) *Protein Sci. 4*, 1955−1965.
39. Loll, P. J., Quirk, S., Lattman, E. E., and Garavito, R. M. (1995) *Biochemistry 34*, 4216−4324.
40. Mancia, F., Keep, N. H., Nakagawa, A., Leadlay, P. F., McSweeney, S., Rasmussen, B., Bösecke, P., Diat, O., and Evans, P. R. (1996) *Structure 4*, 339−350.
41. Jönsson, B. M., Håkansson, K., and Liljas, A. (1993) *FEBS Lett. 322*, 186−190.
42. Håkansson, K., and Wehnert, A. (1992) *J. Mol. Biol. 228*, 1212−1218.
43. Xue, Y., Vidgren, J., Svensson, L., Liljas, A., Jonsson, B., and Lindskog, S. (1993) *Proteins 15*, 80−87.
44. Liang, J. Y., and Lipscomb, W. N. (1987) *Biochemistry 26*, 5293−5301.
45. Merz, K. M., and Banci, L. (1997) *J. Am. Chem. Soc. 119*, 863−871.
46. Lindskog, S., and Liljas, A. (1993) *Curr. Opin. Struct. Biol. 3*, 915−920.
47. Lindskog, S. (1997) *Pharmacol. Ther. 74*, 1−20.
48. Liljas, A., Håkansson, K., Jonsson, B. H., and Xue, Y. (1994) *Eur. J. Biochem. 219*, 1−10.
49. Garmer, D., and Krauss, M. (1992) *J. Am. Chem. Soc. 114*, 6487−6493.
50. Bacon, D., and Anderson, W. F. (1988) *J. Mol. Graphics 6*, 219−220.
51. Merritt, E. A., and Murphy, M. E. P. (1994) *Acta Crystallogr. D50*, 869−873.
52. Sharp, K., Fine, R., and Honig, B. (1987) *Science 236*, 1460−1463.
53. Cruickshank, D. W. J. (1999) *Acta Crystallogr. D55*, 583−601.
54. Kimber, M. S., and Pai, E. F. (2000) *EMBO J. 19*, 1407−1418.

BI000204S